^{1}H$-^{13}$C/^{1}H$-^{15}$N Heteronuclear Dipolar Recoupling by R-Symmetry Sequences Under Fast Magic Angle Spinning for Dynamics Analysis of Biological and Organic Solids

Guangjin Hou,[†,‡] In-Ja L. Byeon,[‡,§] Jinwoo Ahn,[‡,§] Angela M. Gronenborn,[‡,§] and Tatyana Polenova*,[†,‡]

[†]Department of Chemistry and Biochemistry, University of Delaware, Newark, Delaware 19716, United States

[‡]Pittsburgh Center for HIV Protein Interactions, University of Pittsburgh School of Medicine, 1051 Biomedical Science Tower 3, 3501 Fifth Avenue, Pittsburgh, Pennsylvania 15261, United States

[§]Department of Structural Biology, University of Pittsburgh School of Medicine, 1051 Biomedical Science Tower 3, 3501 Fifth Avenue, Pittsburgh, Pennsylvania 15261, United States

S *Supporting Information*

ABSTRACT: Fast magic angle spinning (MAS) NMR spectroscopy is becoming increasingly important in structural and dynamics studies of biological systems and inorganic materials. Superior spectral resolution due to the efficient averaging of the dipolar couplings can be attained at MAS frequencies of 40 kHz and higher with appropriate decoupling techniques, while proton detection gives rise to significant sensitivity gains,

therefore making fast MAS conditions advantageous across the board compared with the conventional slow- and moderate-MAS approaches. At the same time, many of the dipolar recoupling approaches that currently constitute the basis for structural and dynamics studies of solid materials and that are designed for MAS frequencies of 20 kHz and below, fail above 30 kHz. In this report, we present an approach for ^{1}H$-^{13}$C/^{1}H$-^{15}$N heteronuclear dipolar recoupling under fast MAS conditions using R-type symmetry sequences, which is suitable even for fully protonated systems. A series of rotor-synchronized R-type symmetry pulse schemes are explored for the determination of structure and dynamics in biological and organic systems. The investigations of the performance of the various RN$_n^v$-symmetry sequences at the MAS frequency of 40 kHz experimentally and by numerical simulations on [U-^{13}C,^{15}N]-alanine and [U-^{13}C,^{15}N]-*N*-acetyl-valine, revealed excellent performance for sequences with high symmetry number ratio ($N/2n > 2.5$). Further applications of this approach are presented for two proteins, sparsely ^{13}C/uniformly ^{15}N-enriched CAP-Gly domain of dynactin and U-^{13}C,^{15}N-Tyr enriched C-terminal domain of HIV-1 CA protein. Two-dimensional (2D) and 3D R16$_3^2$-based DIPSHIFT experiments carried out at the MAS frequency of 40 kHz, yielded site-specific ^{1}H$-^{13}$C/^{1}H$-^{15}$N heteronuclear dipolar coupling constants for CAP-Gly and CTD CA, reporting on the dynamic behavior of these proteins on time scales of nano- to microseconds. The R-symmetry-based dipolar recoupling under fast MAS is expected to find numerous applications in studies of protein assemblies and organic solids by MAS NMR spectroscopy.
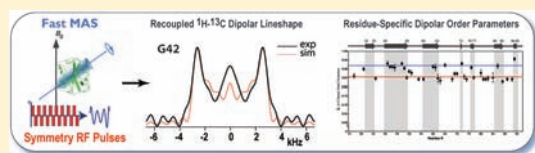
■ INTRODUCTION

Solid-state NMR spectroscopy has emerged as a powerful method for determination of molecular structure and dynamics in biological solids and materials, especially since the advent of magic angle spinning (MAS) in 1950s by Andrew[1] and independently by Lowe.[2] Various anisotropic spin interactions can be averaged out partly or completely by a rapid rotation of a solid sample around the "magic angle" axis, giving rise to greatly enhanced sensitivity and resolution and yielding liquidlike spectra.[1−3] This suppression of the anisotropic portions of spin interactions, while necessary and advantageous from the resolution and sensitivity standpoints, results in a loss of valuable information about the geometric and electronic structure of the solid under investigation. Therefore, multiple laboratories have focused efforts on development of recoupling methods that permit measurements of the anisotropic interactions under MAS conditions in order to gain structural and dynamics information.[4−28]

The majority of the currently existing recoupling techniques perform best at moderate MAS frequencies, below 20 kHz.

With the breakthroughs in the MAS probe technology starting in the late 1990s, fast MAS frequencies of the order of 40−70 kHz are now accessible to an NMR spectroscopist.[29,30] These fast MAS conditions result in greatly enhanced spectral resolution due to the efficient suppression of homonuclear ^{1}H$-^1$H dipolar interactions at frequencies above 40 kHz.[31−33] Moreover, under fast MAS conditions, proton-detected experiments have become a reality in uniformly isotopically enriched proteins. Proton detection provides further benefits due to both several-fold sensitivity increase compared with the heteronucleus detection and the additional information gained by incorporating the ^{1}H dimension into the spectra.[32−36] With these advances, detailed structural

and dynamics analysis of very large proteins and protein assemblies containing either uniform or dilute isotopic labels is now becoming feasible.[37−42] Therefore, development of recoupling protocols that work under fast MAS conditions becomes particularly important at this time. Specifically, measurement of heteronuclear (^{1}H−^{13}C and ^{1}H−^{15}N) dipolar couplings is critical as these couplings provide structural and dynamics information in a broad range of systems, such as proteins, biopolymers, and organic solids. To date several recoupling schemes have been established for correlation spectroscopy under fast MAS frequencies;[43−52] however, to the best of our knowledge, heteronuclear dipolar recoupling methodology for recording ^{1}H−^{13}C and/or ^{1}H−^{15}N dipolar couplings in fully protonated solids under these conditions is still under development. Recently, a REDOR-based measurement of ^{1}H−^{15}N order parameters in a highly deuterated microcrystalline ubiquitin has been reported.[53,54] This approach requires extensive deuteration of the protein under study because REDOR-based field irradiation cannot suppress ^{1}H−^{1}H homonuclear dipolar couplings in highly protonated systems, even under fast MAS conditions.

Recently, Levitt and co-workers presented the generalized symmetry theorems[55,56] that are very useful in the design of radio frequency (RF) schemes for selective recoupling and/or decoupling of the various anisotropic spin interactions in MAS NMR spectroscopy.[17,18,20,57−63] Such symmetry-based approaches are classified by Levitt as CN_n^ν and RN_n^ν recoupling schemes, where the symbols N, n, and ν are small integers and are referred to as the symmetry numbers of the pulse sequence, depending on the rotation properties of the spin angular momenta during the rotor-synchronized train of radio frequency (RF) pulses. Comparing these two classes of symmetry-based schemes, the R-type sequences have more restrictive selection rules than the C-type sequences.[20,55−57] Our analysis of the Hamiltonians corresponding to the various anisotropic spin interactions suggests that it is possible to selectively reintroduce heteronuclear (^{1}H−^{13}C/^{1}H−^{15}N) dipolar interactions by appropriately designed RN_n^ν symmetry pulse sequences while suppressing homonuclear dipolar couplings, even under fast MAS conditions. Here, we present a series of rotor-synchronized RN_n^ν symmetry pulse schemes, as shown in Table S1 in the Supporting Information (SI), suitable for the determination of heteronuclear dipolar couplings under a wide range of MAS frequencies, including fast MAS conditions. These sequences are highly effective in suppressing ^{1}H−^{1}H homonuclear dipolar couplings, which makes them suitable for dipolar recoupling in fully protonated systems. Dipolar truncation for the different heteronuclear spin pairs suppresses the influence of remote protons and ^{1}H chemical shift anisotropy (CSA) on the spectra. These R-type symmetry sequences are employed in this work for the measurement of ^{1}H−^{13}C and ^{1}H−^{15}N dipolar couplings, which bear crucial structural and dynamics information in biological and organic solids. We first evaluate the performance of these RN_n^ν symmetry sequences experimentally and by numerical simulations at the MAS frequency of 40 kHz in [U-^{13}C,^{15}N]-alanine and [U-^{15}N]-N-acetyl-valine (NAV). We next demonstrate the applications of these sequences in [U-^{13}C/^{15}N]-Tyr-labeled C-terminal domain of HIV-1 CA protein and in [sparsely ^{13}C/U-^{15}N]-labeled CAP-Gly domain of dynactin, where we have measured ^{1}H−^{13}C$^\alpha$ dipolar couplings in a site-specific way. The results indicate the high accuracy and precision of the derived heteronuclear dipolar couplings. The approach presented in this report is anticipated to be broadly applicable to determination of heteronuclear dipolar

couplings in organic solids and biological systems, such as proteins, protein assemblies, and nucleic acids, under a variety of MAS conditions including both fast and moderate spinning frequencies.

■ EXPERIMENTS AND METHODS

Materials. U-^{13}C,^{15}N-labeled L-alanine and U-^{15}N-labeled N-acetyl-valine (NAV) were purchased from Cambridge Isotope Laboratories and used without further purification. Both powder samples were packed into the 1.8 mm MAS rotors for subsequent NMR experiments. The conical assemblies of U-^{13}C,^{15}N-tyrosine-labeled C-terminal domain (CTD) of HIV-1 CA capsid protein were prepared by controlled precipitation from 50% w/v solution of PEG-4000 at the ratio of 1:1 (v/v) with the final concentration of 16 mg/mL, followed by incubation at 37 °C for 1 h, as reported previously.[42] CAP-Gly sparsely enriched in ^{13}C and uniformly labeled with ^{15}N was prepared from E. coli, grown in a minimal medium containing 1,3-^{13}C glycerol (Cambridge Isotope Laboratories) as the sole carbon source and ^{15}NH$_4$Cl as the sole nitrogen source. The solid-state NMR sample of CAP-Gly was prepared by controlled precipitation from polyethylene glycol, by slowly adding a solution of 30% PEG-3350 to the solution of 24.3 mg of CAP-Gly (38.5 mg/mL), both dissolved in 10 mM MES buffer (10 mM MgCl$_2$, pH 6.0), as described previously.[64]

Solid-State NMR Spectroscopy. All NMR experiments were recorded on a Varian InfinityPlus solid-state NMR spectrometer, operating at a Larmor frequency of 599.8 MHz for ^{1}H, 150.8 MHz for ^{13}C, and 60.8 MHz for ^{15}N. A 1.8-mm MAS triple-resonance probe developed in the Samoson laboratory was used (spinning rates up to 50 kHz). All samples were packed into 1.8-mm rotors, and all spectra were recorded at a MAS frequency of 40 kHz, controlled to within ±5 Hz. The typical 90° pulse length was 2.8 μs (^{1}H), 4.1 μs (^{13}C), and 7 μs (^{15}N). The temperature was calibrated at different MAS frequencies using a PbNO$_3$ temperature sensor,[65] and the actual temperature at the sample was maintained to within ±0.5 °C throughout the experiments using the Varian temperature controller.

For NMR experiments on Ala and NAV, a 2D DIPSHIFT sequence shown in Figure 1a was used. To reduce the sample heating during fast MAS, nitrogen gas was used for cooling, resulting in a final sample temperature of 20 °C for the Ala and NAV samples. TPPM ^{1}H decoupling with a weak RF field strength[66] of 11 kHz was used during the acquisition period t_2, and CW decoupling with the same RF field strength was applied the duration $T − t_1$. The ^{1}H−^{13}C(^{15}N) cross-polarization was performed with a linear amplitude ramp (80−100%) on ^{13}C(^{15}N); the ^{1}H radio frequency field was 55 kHz with the center of ramp Hartmann−Hahn matched to the first spinning sideband. The contact time was 1.5 ms, and the recycle delay was 5.0 s. A series of 2D NMR spectra were recorded with different RN_n^ν symmetry pulse irradiation applied during t_1. The basic R element was a π pulse; the RF field strength ($N/2n \cdot \omega_R$) and the phase ($\pm\nu/N \cdot 180°$) for each symmetry sequence are determined by its symmetry properties, as shown in Figure S1, SI. The ^{1}H RF field strengths were 112 kHz for R28$_5^4$, 110 kHz for R22$_4^3$, 106.7 kHz for R16$_3^2$, 104 kHz for R26$_5^3$, 93.3 kHz for R14$_3^1$, 90.0 kHz for R18$_4^1$, 88.0 kHz for R22$_5^1$, 86.7 kHz for R26$_6^1$, 80.0 kHz for R4$_1^4$, 74.3 kHz for R26$_7^1$, and 72.0 kHz for R18$_5^1$ dipolar recoupling period. Each RF field strength ($N/2n \cdot \omega_R$) was optimized directly on the detected sample by finding the "zero" point for the fixed-length π pulse ($\nu^* \tau_R/N$). Sixteen scans were accumulated for each t_1 increment, and a total of 32 t_1 increments were recorded for each spectrum. It is worth noting that, despite the high RF field strengths employed during the R-based recoupling period, RF heating is not a problem in any of the samples of interest including proteins, due to short irradiation times, the longest recoupling period being 1.2 ms.
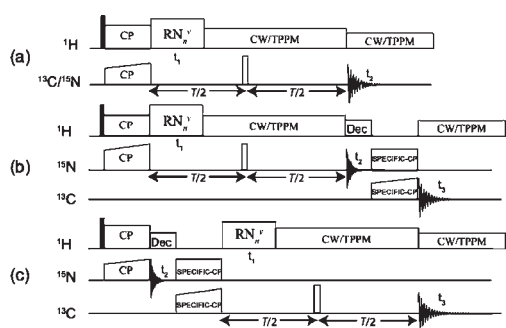
Figure 1. (a) Two-dimensional (2D) and (b, c) three-dimensional (3D) DIPSHIFT pulse sequences for $^1H-^{13}C$ or $^1H-^{15}N$ heteronuclear dipolar recoupling experiments under fast MAS conditions (frequencies of 40 kHz or above). RF irradiation consisting of RN_n^v symmetry pulses is applied on proton spins during the t_1 time to reintroduce the $^1H-^{15}N$ (b) or $^1H-^{13}C$ (c) dipolar couplings. In (b, c), SPECIFIC-CP is used to establish NCA or NCO chemical shift correlations. CW or TPPM with weak RF irradiation (typically, 10 kHz) is applied for ^1H dipolar decoupling under fast MAS.

For U-^{13}C,^{15}N-Tyr-labeled CTD capsid protein, 2D $R16_3^2$-based DIPSHIFT experiments were performed for the measurement of $^1H-^{15}N$ and $^1H-^{13}C^\alpha$ heteronuclear dipolar couplings. 6144 scans with a pulse delay of 1.0 s were accumulated for each t_1 increment (dw = 75 us, corresponding to three rotor periods), and a total of 16 t_1 increments were recorded for each spectrum. For sparsely ^{13}C,U-^{15}N-enriched CAP-Gly protein sample, a 3D $^1H-^{13}C$ $R16_3^2$-based DIPSHIFT spectrum was recorded. The pulse sequence is shown in Figure 1(c). TPPM ^1H decoupling was used during the acquisition period t_3, and CW decoupling was used during t_2 and duration $T - t_1$; the decoupling RF field strength was 11 kHz in both cases. During the SPECIFIC-CP period, no ^1H decoupling was applied. A total of 20 t_1 and 36 t_2 increments were used to record the 3D DIPSHIFT spectrum, and 256 scans with a pulse delay of 2.0 s were accumulated for each increment. The total experimental time was 102 h for the 3D DIPSHIFT experiment. For both protein samples, the MAS frequency was set to 40 kHz and was controlled to within ±10 Hz by a Varian MAS controller. To reduce sample heating from fast spinning, nitrogen gas was used for cooling, resulting in a final temperature of −5 °C at the protein sample. ^1H RF field irradiation of 106.7 kHz was used to reintroduce $^1H-^{13}C$ dipolar couplings during the $R16_3^2$-t_1 time. A real acquisition mode was used for the t_1 dipolar dimension in all DIPSHIFT NMR experiments. All 2D and 3D NMR data were processed in NMRPipe in a Mac environment by zero filling and Fourier transformation. In the 3D DIPSHIFT on CAP-Gly protein, linear prediction was also performed in N^{15} (t_2) dimension. The dipolar lineshapes were extracted along the ^{13}C (^{15}N) isotropic chemical shift dimension.

Numerical Simulations. Numerical simulations of $^1H-^{13}C$ and $^1H-^{15}N$ dipolar spectra were performed using the SIMPSON software package.[67] Nine hundred and eighty-six ZCW angles (α, β) and 3 γ angles were used to generate a powder average for all γ-encoded R-type symmetry sequences. Nine hundred and eighty-six ZCW angles (α, β) and 64 γ angles were employed for non-γ-encoded $R4_1^4$ symmetry sequence. For extracting the best-fit dipolar patterns, the same experimental parameters (i.e., ^1H Larmor frequency, MAS frequency, RF field strength, number of t_1 points, finite pulse lengths, zero-filling, line broadening, etc.) were used in the simulations for each experiment. SIMPLEX method was followed for the fitting of $^1H-^{15}N$ and $^1H-^{13}C$ dipolar lineshapes, whereas effective χ^2 values were calculated following a simplified protocol embedded in SIMPSON-Minuit, assuming that the invidual points of the experimental dipolar line shape display the same variance. We note that for dipolar spectra this procedure results in higher

χ^2 values than those generated in the noise-weighted χ^2 calculation, because of the overestimated contributions of the outer (low-intensity) regions of the dipolar spectrum to the overall powder pattern. Thus, the effective χ^2 values presented in this report are higher (errors are over-estimated) than the actual errors. Isolated H−N and H−C spin pairs were used in the simulations, and the effect of ^1H chemical shift anisotropy was taken into account as well (δ_σ = 10.0 ppm and $\eta = 1$ for the NH proton, δ_σ = 2.0 ppm and $\eta = 1$ for the CH proton; the principal element, δ_{zz}, was assumed to lie along the dipolar vector). The best fit parameters, including dipolar coupling constant (ω_D) and Lorentzian line broadening (LB), were extracted from the simulated dipolar line shape possessing the lowest χ^2.

■ RESULTS AND DISCUSSION

Symmetry-Based Sequences for Heteronuclear Dipolar Recoupling at Fast MAS: General Properties and Numerical Simulations. The generalized pulse sequence for R-symmetry-based 2D separated local field (SLF)[20,21,68−70] spectroscopy is shown in Figure 1a. Following the ramped cross-polarization (CP)[71] period, the CP-enhanced $^{13}C/^{15}N$ magnetization evolves for a constant duration T, with a π pulse inserted at $T/2$ to refocus the $^{13}C/^{15}N$ isotropic chemical shift. Simultaneously, the MAS-averaged $^1H-^{13}C$ or $^1H-^{15}N$ dipolar couplings are reintroduced during the variable evolution period, t_1, by a rotor-synchronized RN_n^v RF pulse train on ^1H spins, followed by ^1H heteronuclear decoupling applied for the duration, $T - t_1$. In order to provide an additional chemical shift dimension, necessary for the applications of this approach to uniformly or extensively ^{13}C,^{15}N-enriched proteins and protein assemblies, the SPECIFIC CP sequence[72] can be used to establish NCA or NCO correlations either following or preceding the RN_n^v dipolar and ^{15}N chemical shift evolution periods, as shown in Figure 1b and c, respectively. The resulting 3D spectrum contains either $^1H-^{15}N$ (Figure 1b) or $^1H-^{13}C$ (Figure 1c) dipolar lineshapes for each residue along the t_1 dimension, and the corresponding ^{15}N and ^{13}C isotropic chemical shifts along the t_2 and t_3 dimensions. Under fast MAS conditions, no ^1H decoupling is necessary during the SPECIFIC-CP period, and the maximum DCP transfer efficiency is achieved.

The R-type symmetry sequences suitable for dipolar recoupling at fast MAS frequencies of 40 kHz or above are summarized in the SI (see Table S1). These particular schemes are chosen to satisfy the typical NMR hardware requirements and limitations in a modern spectrometer (i.e., the maximum ^1H RF field strength achievable in a typical MAS probe, as well as the amplifier RF power limitations), and to yield the optimal (highest possible) scaling factor[55,58] for the dipolar recoupling. The symmetry numbers of the sequences listed in Table S1, SI, are limited to the range $10 \leq N \leq 30$, and the ratios of the symmetry numbers are limited to $1.0 < N/2n \leq 5.0$, to yield RF powers compatible with the available modern hardware. All of the symmetry sequences under discussion except for $R4_1^4$ are γ-encoded, and as shown below, all of them exhibit excellent performance in recoupling heteronuclear dipolar Hamiltonian interactions while suppressing the first-order homonuclear dipolar Hamiltonian to zero, with simultaneous efficient reduction of the recoupled second-order Hamiltonian terms H_{DD-DD} and H_{DD-CSA}. The recoupled heteronuclear dipole−dipole Hamiltonian terms can be characterized by four quantum numbers $\{l, m, \lambda, \mu\}$, and the γ-encoded RN_n^v symmetry sequences can be divided into two categories on the basis of their recoupling properties with respect

to particular Hamiltonian terms. The Hamiltonian terms corresponding to $\{l, m, \lambda, \mu\} = \{2, 2, 1, -1\}$ and $\{2, -2, 1, 1\}$ are recoupled by γ-encoded RN_n^ν symmetry sequences with $N > 2n$, and the Hamiltonian terms with $\{l, m, \lambda, \mu\} = \{2, 2, 1, 1\}$ and $\{2, -2, 1, -1\}$ are recoupled by γ-encoded RN_n^ν symmetry sequences with $N < 2n$. Each symmetry sequence exhibits different scaling factor for recoupling heteronuclear dipolar interactions, and generally the symmetry sequences with higher N/n ratio have larger scaling factors (as shown in Figure S2 of the SI). The RF field strength required for the RN_n^ν symmetry sequences consisting of π pulses as basic R elements is dependent on the symmetry numbers and MAS frequency, $\omega_1 = N\omega_R/2n$.

In this work, we employed the simplest π pulse as the basic R element for all RN_n^ν sequences, and the RF field applied on the proton spins equals $N/2n$ times the MAS frequency, as illustrated in Table S1, SI. For the various RN_n^ν symmetry sequences presented in Figure 1, we have simulated the $^1\text{H}-^{15}\text{N}$ and $^1\text{H}-^{13}\text{C}$ dipolar patterns for the MAS frequency of 40 kHz, and the resulting lineshapes are illustrated in Figure S3 of the SI. These simulated spectra suggest that R-type symmetry sequences should work well for heteronuclear dipolar recoupling spectroscopy under fast MAS conditions, and that the dipolar couplings can be extracted from the overall line shape. In these simulations, we assumed an isolated H—N spin system, and the resulting lineshapes are identical for all RN_n^ν sequences, except being scaled by sequence-specific scaling factors. These scaling factors differ depending on the sequence, and notably, the $R4_1^4$ (rotary resonance, $n = 2$) sequence displays the highest scaling factor, ~ 0.5, almost 1.6 times as large as the highest scaling factor for other γ-encoded R-symmetry sequences that were considered here. A total of six first-order heteronuclear dipole—dipole Hamiltonian terms, $\{l, m, \lambda, \mu\} = \{2, \pm 2, 1, -1\}$, $\{2, \pm 2, 1, 1\}$ and $\{2, \pm 2, 1, 0\}$ are reintroduced by $R4_1^4$ symmetry irradiation under fast MAS frequencies, giving rise to a large scaling factor. However, $R4_1^4$ symmetry scheme is not very effective in suppressing higher-order Hamiltonian terms, and especially higher-order homonuclear dipolar interactions that would affect the line shape of the $^1\text{H}-^{15}\text{N}/^1\text{H}-^{13}\text{C}$ dipolar patterns.

The simulations also revealed that the dipolar line shapes depend to a greater or lesser extent on other spin interactions and experimental imperfections, which include multiple protons, chemical shift anisotropy of protons, and RF field inhomogeneity. Each R-type symmetry sequence has different sensitivity to these factors, as illustrated in Figures S4—S6 of the SI, and a brief discussion follows here.

The effect from remote protons in NHx ($x > 1$) spin system is negligible, demonstrating that all RN_n^ν symmetry sequences, even the non-γ encoded $R4_1^4$, can suppress $^1\text{H}-^1\text{H}$ homonuclear dipolar couplings very efficiently (see Figure S4, SI). Therefore, the R-type symmetry sequences under study are suitable for dipolar recoupling in highly protonated spin systems, because for these sequences the recoupled dipolar Hamiltonian terms do not commute with each other for different spin pairs, and the weak heteronuclear dipolar interactions from remote protons are efficiently suppressed in the presence of the strong one-bond dipolar couplings due to the dipolar truncation effect.

Even though the dipolar recoupling RN_n^ν symmetry sequences reintroduce the chemical shift anisotropy interactions of the irradiated protons, the recoupled ^1H CSA interactions only result in a slight increase of the central peak while the dipolar splitting does not change at all (see Figure S5, SI). We note that ^1H CSA effect could be efficiently suppressed in an alternative approach,

by a modified SLF method, the proton-detected local field (PDLF) approach.[73]

Accurate RF field calibration is required for R-type symmetry sequences due to the repeated "reverse" operations of the individual elements of the R blocks, and the experimental precision would be influenced by the mismatch of the RF field strength (see Figure S6 in the SI). When the phase shift ($2\nu\pi/N$) between the pulse pairs is close to 180°, the influence of the RF field mismatch error is expected to be compensated by the neighboring pairs, which is especially pronounced in sequences with a high symmetry number ratio of N/n, making them the least sensitive to experimental imperfections. In practice, the RF field strength is optimized directly on the sample under investigation by finding the "zero" point when the π pulse duration is set to a fixed value dictated by the particular R-type symmetry, $\nu\tau_R/N$.

It is also important to consider the effect of RF field inhomogeneity on dipolar lineshapes. The inverse operation by R-type element usually requires high RF field homogeneity of NMR probe, otherwise rendering the dipolar measurements inaccurately (see Figure S7, SI). The simulations indicate that the RF inhomogeneity has the most pronounced effect on the non-γ-encoded $R4_1^4$ symmetry sequence, which otherwise would be the most advantageous recoupling scheme due to its highest scaling factor for the recoupling of heteronuclear dipolar interaction. The manifestation of the RF field inhomogeneity is an increase in the intensity of the central peak and a broadening of the dipolar splitting, which become more pronounced with the increasing RF field inhomogeneity. Therefore, $R4_1^4$ symmetry sequence is unsuitable for accurate dipolar coupling measurement in MAS probes possessing low RF field homogeneity (in practice, 85% or lower). The simulations also reveal the fact that for γ-encoded RN_n^ν symmetry sequences, the stronger the RF field ($N\omega_R/2n$) is, the weaker is the effect from RF field inhomogeneity. In practical terms, the above implies that one has to consider the trade-off between the scaling factor and the RF field inhomogeneity of a particular probe. Generally, it is most advantageous to select RN_n^ν symmetry sequences with higher $N/2n$ ratios for determining accurately $^1\text{H}-^{13}\text{C}/^1\text{H}-^{15}\text{N}$ heteronuclear dipolar coupling constants, as long as the required RF field strength ($N\omega_R/2n$) can be attained in the fast MAS probe available to the experimentalist.

Heteronuclear Dipolar Recoupling by R-Symmetry Sequences at Fast MAS Frequencies: Experiments on Alanine and NAV. Guided by the results of numerical simulations, we conducted R-symmetry-based $^1\text{H}-^{13}\text{C}$ dipolar recoupling experiments on a sample of U-^{13}C,^{15}N-labeled L-alanine, spun at the MAS frequency of 40 kHz. Figure 2 shows the $^1\text{H}-^{13}\text{C}$ dipolar lineshapes for CH recorded with (a) $R22_5^1$, (b) $R18_4^1$, (c) $R24_5^2$, (d) $R22_4^3$, (e) $R14_3^1$, (f) $R26_5^3$, (g) $R28_5^4$, and (h) $R16_3^2$ symmetry sequences, respectively. The $^1\text{H}-^{13}\text{C}$ dipolar coupling constants were extracted from numerical simulations of each line shape; the simulated lineshapes are displayed as dotted lines in Figure 2. Similarly, $^1\text{H}-^{13}\text{C}$ dipolar coupling constants for the CH_3 group can be extracted by fitting the corresponding dipolar line shapes recoupled by the various RN_n^ν symmetry sequences (see Figure S8 in the Supporting Information). Several important conclusions can be drawn on the basis of the results.

First, the dipolar coupling constants derived from the different R-symmetry sequences are in excellent agreement within each type of carbon environment, CH and CH_3. As anticipated, the dipolar couplings for the CH groups correspond to the rigid limit
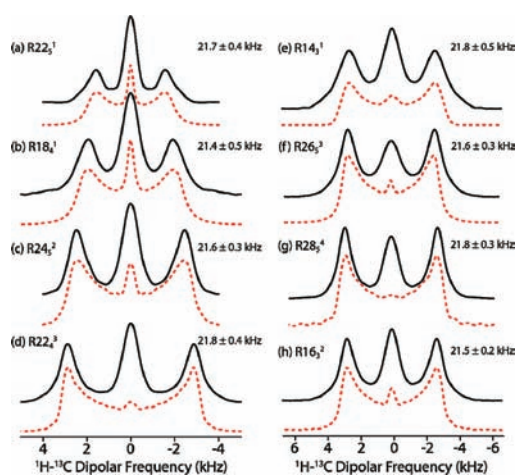
Figure 2. [Black solid lines]: experimental $^1H-^{13}C$ dipolar lineshapes of the CH groups in U-^{13}C,^{15}N-alanine recorded at the MAS frequency of 40 kHz using (a) $R22_5^1$, (b) $R18_4^1$, (c) $R24_5^2$, (d) $R22_4^3$, (e) $R14_3^1$, (f) $R26_5^3$, (g) $R28_5^4$, and (h) $R16_3^2$ symmetry sequences. During the dipolar evolution period t_1, the ^1H RF field irradiation strength is 88, 90, 96, 110, 93.3, 104, 112, and 106.7 kHz for (a−h), respectively. [Red dashed lines]: simulated best-fit $^1H-^{13}C$ dipolar lineshapes. The dipolar coupling constants extracted from the experimental lineshapes are indicated next to each spectrum.

case, with $\omega_D = 21.7 \pm 0.4$ kHz and $r_{CH} = 1.105 \pm 0.007$ Å, in excellent agreement with the X-ray structure ($r_{CH} = 1.095 \pm 0.004$).[74]

Second, the dipolar couplings for the CH$_3$ group are smaller ($\omega_D = 7.6 \pm 0.2$ kHz) due to dynamic averaging caused by a three-site hop exhibited by the methyl group. The reorientation of the H−C dipolar vectors due to fast rotation would result in reduced dipolar coupling, which can be expressed as

$$\omega_D^{\text{reduced}} = \frac{3\cos^2\theta - 1}{2}\omega_D^{\text{rigid}} \quad (1)$$

where θ denotes the angle between the H−C dipolar vector and the rotational axis. Considering the three-site hopping motion of −CH$_3$, the expression for the H−C−H angle can be readily derived:

$$\varphi = 2\sin^{-1}\left(\frac{2}{3}\sqrt{2\left(1 - \frac{\omega_D^{\text{reduced}}}{\omega_D^{\text{rigid}}}\right)}\right) \quad (2)$$

According to the motionally averaged H−C dipolar coupling measured in the −CH$_3$ group and assuming the rigid H−C dipolar coupling to be the same as for the −HC group, the calculated H−C−H angle φ is 101.6 ± 2°, which is close to the value of 108.5 ± 0.3° in the reported crystal structure.[75]

Third, the effective scaling factors observed in each experiment follow those predicted by simulations: generally, for γ-encoded heteronuclear dipolar recoupling using symmetry sequences, the higher the ratio of the RF field to the spinning frequency (ω_{1H}/ω_R), the larger the scaling factor. Even though the non-γ-encoded $R4_1^4$ sequence exhibits the highest scaling factor (see Figure S2 in the SI), there exists an intense central peak in the dipolar line shape, which arises from the RF field inhomogeneity, as discussed above. Fourth, the simulated spectra for a four-spin model are consistent with the experimental results, recorded with

various R-symmetry sequences. This indicates that this minimal model is sufficient for capturing the salient spectral features. As discussed above, the central peaks in the experimental dipolar patterns are contributions from RF field inhomogeneity, ^1H chemical shift anisotropy, and the relaxation due to the applied RF field irradiation. Such central peaks are commonly seen in dipolar recoupling experiments,[17,38] and they introduce minor (5−10%) uncertainties in the derived dipolar coupling constants. For all simulations in the current report, the relaxation times were not taken into account.

We also examined the performance of the R-symmetry-based sequences for $^1H-^{15}N$ dipolar recoupling under fast MAS conditions ($\omega_r = 40$ kHz) using [^{15}N]-N-acetyl-valine (NAV) (see Figure S9 in the SI). Similar to the $^1H-^{13}C$ dipolar recoupling experiments, each R-type sequence exhibits a different scaling factor, and among these five sequences, the $R16_3^2$ scheme with RF field strength of 106.7 kHz possesses the highest scaling factor. Unlike the $^1H-^{13}C$ dipolar lineshapes, the $^1H-^{15}N$ dipolar patterns recoupled by $R22_5^1$ and $R18_4^1$ sequences show distortions, possibly caused by the large chemical shift anisotropy (CSA) of the amide proton and RF field inhomogeneity. This feature is also evident in the analysis of the higher-order average Hamiltonian terms containing the recoupled hetero- and homo-nuclear dipole−dipole interactions. These spectral distortions would result in lower precision of the dipolar measurements. Fortunately, these distortions can be suppressed or removed by choosing a suitable RN_n^v symmetry sequence with a higher $N/2n$ ratio, which, in turn, determines the required ratio of the RF field to the spinning frequency (ω_{1H}/ω_R). Indeed, it can be seen that the $^1H-^{15}N$ dipolar patterns recoupled by $R14_3^1$, $R26_5^3$ and $R16_3^2$ symmetry sequences (see Figure S9, SI) suffer much less from distortions caused by RF field inhomogeneity, higher-order Hamiltonian terms, and residual $^1H-^1H$ homonuclear dipolar couplings. The $^1H-^{15}N$ dipolar coupling constants extracted from these experiments are in the range of 9.9 ± 0.3 kHz, corresponding to $r_{NH} = 1.073 \pm 0.003$ Å, in excellent agreement with the expected static-limit H−N bond length. These results demonstrate that higher precision can be attained for the dipolar measurement when sequences with higher symmetry number ratio of N/n are employed, as long as the required RF field strength $N\omega_R/2n$ is permissible in a particular NMR instrument.

We note that, in our current work, we experimentally achieved the highest scaling factor of 0.282 in the $R28_5^4$ sequence (corresponding to the $N/2n$ ratio of 2.8). This corresponds to the RF field strength of 112 kHz at MAS frequency of 40 kHz, which is almost the maximum permissible RF power in our 1.8-mm triple-resonance MAS probe. To the best of our knowledge, many of the modern commercial fast-MAS probes can tolerate much higher ^1H RF field strengths, approximately 200 kHz and possibly even 250 kHz. Under those RF conditions, one can implement other R-symmetry sequences with higher $N/2n$ ratios, including γ-encoded symmetry sequences $R14_2^3$, $R18_2^5$, and $R10_1^3$ that require RF field strengths of 140, 180, and 200 kHz, respectively, when $\omega_R = 40$ kHz. R-symmetry sequences with higher $N/2n$ are beneficial not only because they fully suppress spectral distortions arising from RF field inhomogeneity, higher-order Hamiltonian terms, and $^1H-^1H$ homonuclear dipolar couplings, but also due to their larger scaling factors, i.e. $K_{sc}(R14_2^3) = 0.295$, and $K_{sc}(R10_1^3) = 0.307$. Generally, in order to determine accurately $^1H-^{13}C/^1H-^{15}N$ heteronuclear dipolar couplings under fast or ultrafast MAS conditions by γ-encoded
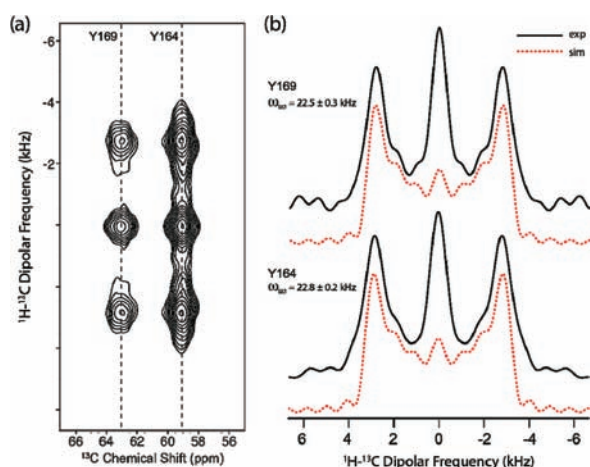
Figure 3. (a) Two-dimensional $^1H-^{13}C$ $R16_3^2$-based DIPSHIFT spectrum of [U-^{13}C,^{15}N]-Tyr HIV-1 C-terminal domain (CTD) of CA protein recorded at the MAS frequency of 40 kHz. The pulse sequence for this spectrum is shown in Figure 1a. (b) [Solid lines]: experimental $^1H-^{13}C^\alpha$ dipolar lineshapes extracted along the ω_1 dimension of the 2D DIPSHIFT spectra. [Dashed lines]: best-fit simulated $^1H-^{13}C^\alpha$ dipolar lineshapes. The experimental and simulated dipolar lineshapes correspond to the two tyrosine residues, Y169 and Y164, and the resulting dipolar coupling constants are 22.5 ± 0.3 and 22.8 ± 0.2 kHz, respectively.

R-type symmetry sequences, RN_n^ν schemes with the ratio of $N/2n > 2.5$ are preferred.

Heteronuclear Dipolar Recoupling by R-Symmetry Sequences at Fast MAS: Applications to Proteins and Protein Assemblies. The fast MAS dipolar recoupling methods described above are particularly advantageous for structural and dynamics characterization of uniformly and sparsely enriched proteins and protein assemblies. We have examined the performance of the R-symmetry-based recoupling sequences under fast MAS conditions for the recoupling of $^1H-^{15}N$ and $^1H-^{13}C$ dipolar interactions in U-^{13}C,^{15}N-Tyr-enriched C-terminal domain (CTD) of HIV-1 CA capsid protein and sparsely ^{13}C/U-^{15}N-labeled 89-residue CAP-Gly domain of dynactin.

The C-terminal domain of HIV-1 CA protein contains three tyrosine residues, Y145, Y164, and Y169, Y164, and Y169 are located in α-helices, while Y145 occupies a pivotal position in the hinge region connecting the C- and N-terminal domains of CA. The hinge region is conformationally flexible,[76,77] and this conformational flexibility might in turn determine the intermolecular packing of the full-length CA proteins in the assembled state, dictating their assembly into different morphologies (i.e., conical, tubular, and spherical). It is therefore of interest to address the structure and internal dynamics on different time scales of Y145 in CTD as well as in the full-length assembled CA protein of different morphologies.

In Figure 3a, a 2D $^1H-^{13}C$ DIPSHIFT spectrum of HIV-1 CTD, recorded at the MAS frequency of 40 kHz, is shown. During the t_1 evolution period, $R16_3^2$ symmetry scheme with a RF field strength of 106.7 kHz was used for reintroducing the $^1H-^{13}C$ dipolar couplings under fast MAS conditions. Y164 and Y169 residues yield two well-resolved $^{13}C^\alpha$ peaks. The Y145 C^α peak is missing, which can be due to dynamics on micro- to millisecond time scales interfering with either cross-polarization or dipolar recoupling. The $^{13}C^\alpha$ chemical shifts for Y164 (59.0 ppm) and Y169 (63.1 ppm) are in excellent agreement with solution
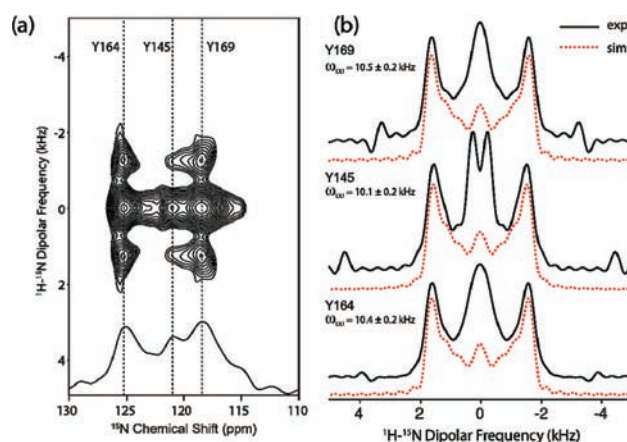

Figure 4. (a) Two-dimensional $^1H-^{15}N$ $R16_3^2$-based DIPSHIFT spectrum of [U-^{13}C,^{15}N]-Tyr HIV-1 C-terminal domain (CTD) of CA protein recorded at the MAS frequency of 40 kHz. The pulse sequence for this spectrum is shown in Figure 1(a). (b) [Solid lines]: Experimental $^1H-^{15}N$ dipolar lineshapes extracted along the ω_1 dimension of the 2D DIPSHIFT spectra. [Dashed lines]: Best-fit simulated $^1H-^{15}N$ dipolar lineshapes. The experimental and simulated dipolar lineshapes correspond to the three tyrosine residues, Y169, Y164, and Y145, and the resulting dipolar couplings are 10.5 ± 0.2, 10.4 ± 0.2, and 10.1 ± 0.2 kHz, respectively.

NMR shifts (59.495 ppm and 63.234 ppm for Y164 and Y169, respectively).[78] In Figure 3b, the experimental (solid lines) and best-fit simulated (dashed lines) $^1H-^{13}C^\alpha$ dipolar patterns for Y164 and Y169 are presented. The experimental $^1H-^{13}C^\alpha$ dipolar lineshapes were extracted along the ^{13}C isotropic chemical shift of each residue. Due to the high RF field homogeneity of ~90% in our 1.8-mm triple-resonance MAS probe (see Figure S10 in the SI), the detected dipolar line shapes were barely affected by RF field inhomogeneity, especially for the R-type symmetry sequences with higher ratio of $N/2n$ (see Figure S7, SI). Therefore, the RF field imperfection was not taken into account for any of the protein line shape fittings. Since the dipolar splitting is determined to the largest extent by the size of the dipolar coupling constants, the best-fit line shape can be readily derived, using the minimal least-squares error criterion, χ^2, as described in the Experiments and Methods section, or even by visual inspection of the line shapes. Dipolar coupling constant (ω_D) and Lorentzian line broadening (LB) are the only two variable parameters. The central part is excluded from the curve fitting when minimizing χ^2, due to its complex dependence on multiple factors. The best-fit spectra shown by the dashed curves in Figure 3, correspond to the minimum χ^2. The fit parameters as well as the uncertainty errors are derived using the SIMPLEX method, as shown in Figure S11 of the SI depicting a χ^2 contour plot for the $^1H-^{13}C$ dipolar line shape fitting of Tyr-164, from which the best fit values of ω_D = 22.8 ± 0.3 kHz and LB = 573 ± 112 Hz are extracted corresponding to the minimum χ^2 of 0.67. As anticipated, Y164 and Y169 exhibit $^1H-^{13}C^\alpha$ dipolar couplings of 22.8 ± 0.3 and 22.5 ± 0.2 kHz, respectively, which is close to the rigid limit value of 22.8 kHz.

We have also carried out $^1H-^{15}N$ $R16_3^2$-based DIPSHIFT measurements in HIV-1 CTD protein, and the results are shown in Figure 4. In this experiment, the peak for Y145 is present, and the ^{15}N chemical shift is 121.1 ppm. The chemical shifts for Y164 (125.2 ppm) and Y169 (118.3 ppm) agree to within ±1.0 ppm with the corresponding solution NMR shifts (124.243 ppm for Y164
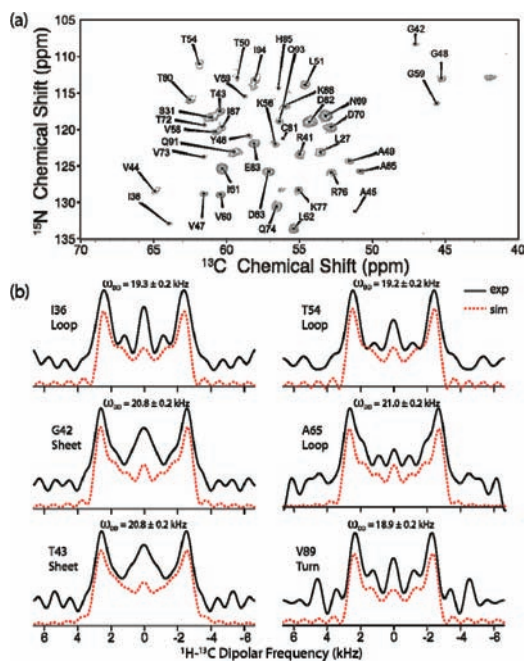
18651

dx.doi.org/10.1021/ja203771a |*J. Am. Chem. Soc.* 2011, 133, 18646–18655

Figure 5. (a) First 2D NCA plane extracted from the 3D $^1H-^{13}C$ $R16_3^2$-based DIPSHIFT spectrum of sparsely $^{13}C/U-^{15}N$-labeled CAP-Gly domain of dynactin. The sample was spun at the MAS frequency of 40 kHz. The pulse sequence for this spectrum is shown in Figure 1c. (b) Representative $^1H-^{13}C^\alpha$ dipolar lineshapes extracted along the ω_1 dimension for the following residues: I36 (loop), G42 (β-strand), T43 (β-strand), T54 (loop), A65 (loop), and V89 (terminus of a β-strand). The best-fit $^1H-^{13}C^\alpha$ dipolar coupling constants are shown above the corresponding dipolar patterns.

Figure 6. Experimental $H-C^\alpha$ dipolar order parameters plotted as a function of the residue number for the sparsely $^{13}C,U-^{15}N$-enriched CAP-Gly protein. The dipolar order parameters were calculated according to the static limit $H-C$ dipolar coupling constant of 22.8 kHz. The blue and red dotted lines correspond to the $H-C^\alpha$ dipolar order parameters of 0.919 and 0.854, which are the average order parameters for the residues comprising β-sheets and loops/turns, respectively.

and 117.738 for Y169). This small discrepancy between the ^{15}N solution- and solid-state chemical shifts is consistent with multiple previous studies of other proteins.[79−81] The $^1H-^{15}N$ dipolar lineshapes were extracted along the ^{15}N isotropic chemical shift of each residue, as shown by the solid lines in Figure 4b. The best-fit simulated lineshapes are shown by the dashed lines in Figure 4b. The $^1H-^{15}N$ dipolar couplings obtained from the numerical simulations are 10.1 ± 0.2 kHz for Y145, 10.4 ± 0.2 kHz for Y164, and 10.5 ± 0.2 kHz for Y169. It can be seen that the $^1H-^{15}N$ dipolar couplings for the three tyrosines are close to the rigid-limit value of 11.34 kHz, even though Y145 has a slightly reduced value.

Both $^1H-^{13}C$ and $^1H-^{15}N$ dipolar couplings are sensitive to motions occurring on time scales of $10^{-9}-10^{-6}$ s. The $^1H-^{15}N$ DIPSHIFT measurement did not reveal significant averaging of the corresponding dipolar interaction for Y145, indicating that the backbone nitrogen is rigid on time scales faster than $\sim10^{-6}$ s. Coupled with the observations of the conformational flexibility of the hinge region by X-ray crystallography[76,77] our solid-state NMR results suggest that motions, if indeed present, have to occur on time scales slower than 10^{-6} s. Detailed dynamics studies of CA protein on multiple time scales are currently in progress in our laboratory.

Figure 5 demonstrates the site-resolved measurement of the $^1H-^{13}C$ dipolar couplings through a 3D DIPSHIFT/SPECI-FIC-CP experiment in the sparsely $^{13}C/U-^{15}N$-labeled 89-residue CAP-Gly domain of dynactin, performed at the MAS frequency of 40 kHz. Resonance assignments for CAP-Gly were reported by us previously.[64] The pulse sequence for this experiment is
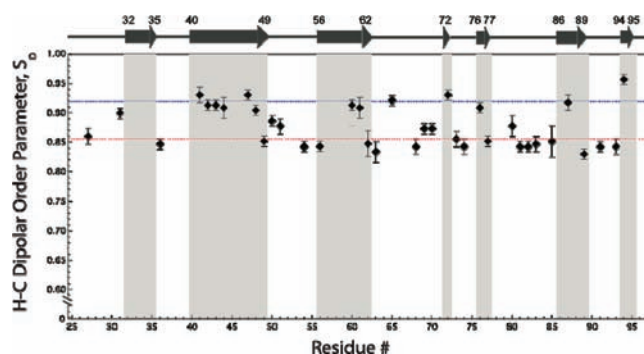
shown in Figure 1c. The γ-encoded $R16_3^2$ symmetry sequence was chosen for $^1H-^{13}C$ dipolar recoupling during the t_1 period due to its high scaling factor and low sensitivity to RF field inhomogeneity, as discussed above. Subsequently, SPECIFIC-CP was employed to establish the NCA correlation after dipolar evolution. The first 2D NCA plane of the 3D DIPSHIFT spectrum is shown in Figure 5a. $^1H-^{13}C^\alpha$ dipolar lineshapes for each residue were extracted along the third dimension, and, with more than 40 peaks resolved in the NCA plane, we obtained a total of 37 dipolar patterns. Examples of $^1H-^{13}C^\alpha$ dipolar lineshapes for six residues, I36, G42, T43, T54, A65, and V89, located in a terminus of a β-strand (one residue), in β-strands (two residues), and in loops (three residues), are shown in Figure 5b. The dipolar coupling constants extracted from these lineshapes by numerical simulations yield important dynamics information, assuming that the static-limit $H-C^\alpha$ dipolar couplings are invariant with the secondary structure, ω_{DD} = 22.8 kHz.[82] The internal motions with correlation times in the range between 10^{-9} and 10^{-6} s result in partial averaging of the anisotropic orientation-dependent dipolar interactions, which manifest themselves in the narrowed dipolar lineshapes. For the above six residues, the dipolar couplings vary, correlating with their different mobility.

Figure 6 shows the $^1H-^{13}C^\alpha$ dipolar order parameters plotted as a function of the residue number (see Table S2, SI, for the ω_{DD} and the minimum χ^2 values for each residue extracted from the fits). These order parameters span the range from 0.83 ± 0.01 to 0.93 ± 0.01, and if we treat the internal mobility of the backbone according to the diffusion-in-a-cone model[83] described in eq 1, the diffusion cone angles for the backbone motions of CAP-Gly would be in the range of 12.5−19.7°. The overall average $H-C^\alpha$ dipolar order parameter is 0.92 ± 0.01 for the observed residues in β-sheets, and 0.85 ± 0.01 for the residues in the loops and termini of β-sheets, as shown in Figure 6 with blue and red dotted lines, respectively. The corresponding $H-C^\alpha$ dipolar coupling constants are 21.0 ± 0.3 and 19.5 ± 0.3 kHz, respectively.

It is important to note that for an overwhelming majority of CAP-Gly residues these dipolar parameters derived from the $R16_3^2$-based DIPSHIFT experiment conducted at the MAS frequency of 40 kHz are in excellent agreement with the parameters recorded by the well-characterized protocol utilizing the $R18_1^7$ sequence at the MAS frequency of 10 kHz (see Figure S12 of
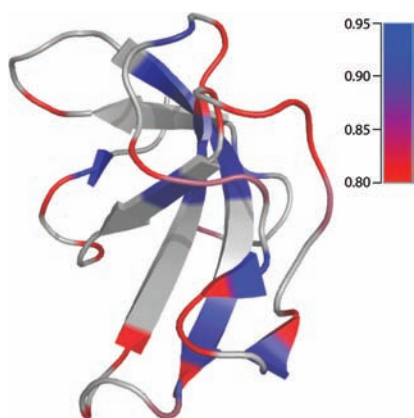
Figure 7. Dynamic behavior of the individual residues in CAP-Gly domain of dynactin on nano- to microsecond time scales mapped onto its tertiary structure, as captured by the experimental ^{1}H$-^{13}$C$^\alpha$ dipolar order parameters, S_D, measured with the R16$_3^2$ symmetry sequence at a fast MAS frequency of 40 kHz. The color scheme is: blue, $S_D = 0.95$, red, $S_D = 0.80$, with continuous interpolation for the values between these limiting order parameters. Shown in gray are residues for which dipolar lineshapes could not be extracted from the spectra due to the congestion of the 2D NCA plane.

the SI), therefore attesting to the accuracy of the R-symmetry-based experiments at fast MAS conditions.

The dynamic behavior of the individual residues in CAP-Gly domain of dynactin captured by ^{1}H$-^{13}$C$^\alpha$ dipolar couplings can be analyzed in the context of its secondary structure. As shown in Figure 7, the individual residues comprising β-sheets exhibit higher dipolar order parameters than the residues located in loops or turns, which generally show lower order parameters presumably due to their mobility on the nano- to microsecond time scales. An interesting exception is A65, which is located in a loop but exhibits a β-sheet-like order parameter as observed in both 40- and 10- kHz DIPSHIFT experiments. The origin of a higher dipolar order parameter for this loop residue needs to be explored in the future. The average reduction in the order parameters for the loop and turn regions of CAP-Gly (regions encompassing A49-K56, L62-T72, K77-H85, V89-Q93) is ∼1.5 kHz compared to the rigid limit values. It should be noted that the average H$-$C$^\alpha$ dipolar order parameters vary in different protein systems, reflecting the extent of the overall backbone mobility of a particular protein. For instance, Lorieau, Day, and McDermott reported the average H$-$C$^\alpha$ dipolar order parameter of 0.99 ± 0.04 in the coat protein of Pf1 bacteriophage.[83] The lower average order parameter value of 0.89 ± 0.01 for CAP-Gly that we observed in the current study is not surprising in light of the higher content of the loop/turn regions. Future studies of a broader range of proteins would be of interest to pursue in order to gain systematic understanding of the internal backbone mobility as a function of the secondary and tertiary structure.

■ CONCLUSIONS

In summary, a series of R-type symmetry sequences have been discussed for the measurements of heteronuclear (^{1}H$-^{15}$N/ ^{1}H$-^{13}$C) dipolar interactions suitable for both fully protonated and deuterated systems under fast MAS frequencies. These symmetry sequences display excellent selectivity for recoupling of the first-order heteronuclear dipolar average Hamiltonian terms while suppressing the homonuclear dipolar Hamiltonian

to zero. In order to suppress the distortions in the dipolar patterns arising from additional spin interactions and experimental hardware imperfections, symmetry sequences with $N/2n$ ratio greater than 2.5 should be used, and these sequences were found to yield more reliable dipolar lineshapes and dipolar coupling constants. The high spectral resolution attained in the multi-dimensional fast-MAS experiments presented in this report, makes this methodology particularly well suited for studies of uniformly, extensively and sparsely enriched proteins and protein assemblies, as we have demonstrated for the CAP-Gly domain of human dynactin and HIV-1 C-terminal domain of CA capsid protein. The measurements revealed that the ^{1}H$-^{15}$N and ^{1}H$-^{13}$C dipolar coupling constants for the Tyr residues in the CA protein do not exhibit any significant reduction with respect to rigid limit values, indicating that the backbone of these residues is rigid on time scales faster than a microsecond. On the other hand, the ^{1}H$-^{13}$C dipolar coupling constants in CAP-Gly vary considerably along the backbone, with residues comprising loops and turns exhibiting reduced dipolar couplings (and dipolar order parameters) and hence mobility higher than that of residues located in β-sheets, on time scales of nano- to microseconds.

We expect that the approach reported here will become indispensible for structural and dynamics characterization of a wide range of systems, from macromolecular systems to organic solids, and will find many interesting applications in chemistry, biology, materials science, and other disciplines.

■ ASSOCIATED CONTENT

Ⓢ Supporting Information. Tables with (i) summary of RN$_n^\nu$ symmetry sequences suitable for heteronuclear dipolar recoupling under fast or ultrafast MAS conditions and (ii) ^{1}H$-^{13}$C$^\alpha$ dipolar coupling constants for each residue in CAP-Gly domain of dynactin, extracted from the 3D R16$_3^2$ DIPSHIFT experiment conducted at 40 kHz. Figures illustrating (1) RN$_n^\nu$ symmetry sequences, (2) effective scaling factors for γ-encoded symmetry sequences plotted as a function of the symmetry numbers, (3) simulated H$-$N and H$-$C dipolar lineshapes recoupled by various symmetry sequences at fast MAS frequency, (4) simulations of the effect of remote protons on H$-$N dipolar lineshapes, (5) simulations of the effect of the ^{1}H CSA on H$-$N dipolar lineshapes, (6) simulations of the effect of RF field mismatch on the accuracy of the dipolar measurement, (7) simulations of the effect of RF field inhomogeneity on H$-$N dipolar lineshapes, (8) experimental ^{1}H$-^{13}$C dipolar lineshapes of CH$_3$ group of U-^{13}C,^{15}N -alanine recorded by various symmetry sequences at MAS frequency of 40 kHz, (9) ^{1}H$-^{15}$N dipolar lineshapes of U-^{13}C,^{15}N$-N$-acetyl-valine recorded by various symmetry sequences at MAS frequency of 40 kHz, (10) the RF field homogeneity profile of our 1.8-mm fast-MAS probe, (11) an example of contour plot for H$-$C dipolar fitting of Y164 in HIV-1 CA protein, (12) the comparison of H$-$C dipolar order parameters in CAP-Gly recorded by R16$_3^2$ sequence at fast MAS frequency of 40 kHz and by R18$_1^7$ sequence at low MAS frequency of 10 kHz. This material is available free of charge via the Internet at http://pubs.acs.org.

■ AUTHOR INFORMATION

Corresponding Author
 tpolenov@udel.edu

■ REFERENCES

(1) Andrew, E. R.; Bradbury, A.; Eades, R. G. *Nature* **1959**, *183*, 1802–1803.

(2) Lowe, I. J. *Phys. Rev. Lett.* **1959**, *2*, 285–287.

(3) McDermott, A. E. *Curr. Opin. Struct. Biol.* **2004**, *14*, 554–561.

(4) Hong, M.; Gross, J. D.; Griffin, R. G. *J. Phys. Chem. B* **1997**, *101*, 5869–5874.

(5) Schmidt-Rohr, K.; Clauss, J.; Spiess, H. W. *Macromolecules* **1992**, *25*, 3273–3277.

(6) Zumbulyadis, N. *Phys. Rev. B* **1986**, *33*, 6495–6496.

(7) Tekely, P.; Nicole, D.; Brondeau, J.; Delpuech, J. J. *J. Phys. Chem.* **1986**, *90*, 5608–5611.

(8) Gullion, T.; Schaefer, J. *J. Magn. Reson.* **1989**, *81*, 196–200.

(9) Tycko, R.; Dabbagh, G. *Chem. Phys. Lett.* **1990**, *173*, 461–465.

(10) Gullion, T.; Vega, S. *Chem. Phys. Lett.* **1992**, *194*, 423–428.

(11) Bennett, A. E.; Ok, J. H.; Griffin, R. G.; Vega, S. *J. Chem. Phys.* **1992**, *96*, 8624–8627.

(12) Bennett, A. E.; Weliky, D. P.; Tycko, R. *J. Am. Chem. Soc.* **1998**, *120*, 4897–4898.

(13) Verel, R.; Ernst, M.; Meier, B. H. *J. Magn. Reson.* **2001**, *150*, 81–99.

(14) Ernst, M.; Bush, S.; Kolbert, A. C.; Pines, A. *J. Chem. Phys.* **1996**, *105*, 3387–3397.

(15) Schnell, I. *Prog. Nucl. Magn. Reson. Spectrosc.* **2004**, *45*, 145–207.

(16) Nielsen, A.; Bjerring, M.; Nielsen, J.; Nielsen, N. *J. Chem. Phys.* **2009**, *131*, 025101.

(17) Hou, G.; Paramasivam, S.; Byeon, I. J.; Gronenborn, A. M.; Polenova, T. *Phys. Chem. Chem. Phys.* **2010**, *12*, 14873–14883.

(18) Chan, J. C. C.; Tycko, R. *J. Chem. Phys.* **2003**, *118*, 8378–8389.

(19) Duma, L.; Abergel, D.; Ferrage, F.; Pelupessy, P.; Tekely, P.; Bodenhausen, G. *Chem. Phys. Chem.* **2008**, *9*, 1104–1106.

(20) Zhao, X.; Eden, M.; Levitt, M. H. *Chem. Phys. Lett.* **2001**, *342*, 353–361.

(21) Levitt, M. H.; Zhao, X.; Sudmeier, J. L.; Bachovchin, W. W. *J. Am. Chem. Soc.* **2001**, *123*, 11097–11098.

(22) Fu, R. Q.; Smith, S. A.; Bodenhausen, G. *Chem. Phys. Lett.* **1997**, *272*, 361–369.

(23) Wei, Y. F.; Lee, D. K.; McDermott, A. E.; Ramamoorthy, A. *J. Magn. Reson.* **2002**, *158*, 23–35.

(24) van Rossum, B. J.; de Groot, C. P.; Ladizhansky, V.; Vega, S.; de Groot, H. J. M. *J. Am. Chem. Soc.* **2000**, *122*, 3465–3472.

(25) Bayro, M.; Ramachandran, R.; Caporini, M.; Eddy, M.; Griffin, R. *J. Chem. Phys.* **2008**, *128*, 052321.

(26) Chou, F.; Huang, S.; Chan, J. C. C. *J. Magn. Reson.* **2009**, *197*, 96–99.

(27) Lewandowski, J. R.; De Paepe, G.; Eddy, M.; Griffin, R. *J. Am. Chem. Soc.* **2009**, *131*, 5769–5776.

(28) Lewandowski, J. R.; De Paepe, G.; Griffin, R. *J. Am. Chem. Soc.* **2007**, *129*, 728–729.

(29) Samoson, A.; Tuherm, T.; Gan, Z. *Solid-State Nucl. Magn. Reson.* **2001**, *20*, 130–136.

(30) Samoson, A.; Tuherm, T.; Past, J.; Reinhold, A.; Anupold, T.; Heinmaa, N. *New Tech. Solid-State NMR* **2005**, *246*, 15–31.

(31) Reif, B.; Jaroniec, C. P.; Rienstra, C. M.; Hohwy, M.; Griffin, R. G. *J. Magn. Reson.* **2001**, *151*, 320–327.

(32) Zhou, D.; Rienstra, C. *Angew. Chem., Int. Ed.* **2008**, *47*, 7328–7331.

(33) Reif, B.; Griffin, R. G. *J. Magn. Reson.* **2003**, *160*, 78–83.

(34) Ishii, Y.; Yesinowski, J. P.; Tycko, R. *J. Am. Chem. Soc.* **2001**, *123*, 2921–2922.

(35) Ishii, Y.; Tycko, R. *J. Magn. Reson.* **2000**, *142*, 199–204.

(36) Zhou, D. H.; Shah, G.; Mullen, C.; Sandoz, D.; Rienstra, C. M. *Angew. Chem., Int. Ed.* **2009**, *48*, 1253–1256.

(37) McDermott, A.; Polenova, T. *Curr. Opin. Struct. Biol.* **2007**, *17*, 617–622.

(38) Yang, J.; Tasayco, M. L.; Polenova, T. *J. Am. Chem. Soc.* **2009**, *131*, 13690–13702.

(39) Thiriot, D. S.; Nevzorov, A. A.; Zagyanskiy, L.; Wu, C. H.; Opella, S. J. *J. Mol. Biol.* **2004**, *341*, 869–879.

(40) Tycko, R. *Prog. Nucl. Magn. Reson. Spectrosc.* **2003**, *42*, 53–68.

(41) Andronesi, O. C.; Pfeifer, J. R.; Al-Momani, L.; Ozdirekcan, S.; Rijkers, D. T.; Angerstein, B.; Luca, S.; Koert, U.; Killian, J. A.; Baldus, M. *J. Biomol. NMR* **2004**, *30*, 253–265.

(42) Han, Y.; Ahn, J.; Concel, J.; Byeon, I. J.; Gronenborn, A. M.; Yang, J.; Polenova, T. *J. Am. Chem. Soc.* **2010**, *132*, 1976–1987.

(43) Brinkmann, A.; Kentgens, A. P. M. *J. Phys. Chem. B* **2006**, *110*, 16089–16101.

(44) Hu, K. N.; Tycko, R. *J. Chem. Phys.* **2009**, *131*, 045101.

(45) Lewandowski, J. R.; De Paepe, G.; Eddy, M. T.; Struppe, J.; Maas, W.; Griffin, R. G. *J. Phys. Chem. B* **2009**, *113*, 9062–9069.

(46) Weingarth, M.; Demco, D. E.; Bodenhausen, G.; Tekely, P. *Chem. Phys. Lett.* **2009**, *469*, 342–348.

(47) Scholz, I.; Huber, M.; Manolikas, T.; Meier, B. H.; Ernst, M. *Chem. Phys. Lett.* **2008**, *460*, 278–283.

(48) Ishii, Y. *J. Chem. Phys.* **2001**, *114*, 8473–8483.

(49) Lange, A.; Scholz, I.; Manolikas, T.; Ernst, M.; Meier, B. H. *Chem. Phys. Lett.* **2009**, *468*, 100–105.

(50) Hou, G.; Yan, S.; Sun, S. J.; Han, Y.; Byeon, I. J.; Ahn, J.; Concel, J.; Samoson, A.; Gronenborn, A. M.; Polenova, T. *J. Am. Chem. Soc.* **2011**, *133*, 3943–3953.

(51) De Paepe, G.; Bayro, M. J.; Lewandowski, J.; Griffin, R. G. *J. Am. Chem. Soc.* **2006**, *128*, 1776–1777.

(52) Brinkmann, A.; Kentgens, A. P. M. *J. Am. Chem. Soc.* **2006**, *128*, 14758–14759.

(53) Ernst, M.; Schanda, P.; Meier, B. H. *J. Magn. Reson.* **2011**, *210*, 246–259.

(54) Schanda, P.; Meier, B. H.; Ernst, M. *J. Am. Chem. Soc.* **2010**, *132*, 15957–15967.

(55) Carravetta, M.; Eden, M.; Zhao, X.; Brinkmann, A.; Levitt, M. H. *Chem. Phys. Lett.* **2000**, *321*, 205–215.

(56) Levitt, M. H. In *Encyclopedia of Nuclear Magnetic Resonance*; Grant, D. M., Harris, R. K., Eds.; Wiley: Chichester, 2002; Vol. 9, pp 165–196.

(57) Eden, M.; Levitt, M. H. *J. Chem. Phys.* **1999**, *111*, 1511–1519.

(58) Brinkmann, A.; Levitt, M. H. *J. Chem. Phys.* **2001**, *115*, 357–384.

(59) Madhu, P. K.; Zhao, X.; Levitt, M. H. *Chem. Phys. Lett.* **2001**, *346*, 142–148.

(60) Bjerring, M.; Nielsen, N. C. *Chem. Phys. Lett.* **2003**, *370*, 496–503.

(61) Eden, M. *Chem. Phys. Lett.* **2003**, *378*, 55–64.

(62) Tycko, R. *J. Chem. Phys.* **2007**, *126*, 064506.

(63) Eden, M.; Lo, A. Y. *J. Magn. Reson.* **2009**, *200*, 267–279.

(64) Sun, S. J.; Siglin, A.; Williams, J. C.; Polenova, T. *J. Am. Chem. Soc.* **2009**, *131*, 10113–10126.

(65) Neue, G.; Dybowski, C. *Solid State Nucl. Magn. Reson.* **1997**, *7*, 333–336.

(66) Ishii, Y.; Kotecha, M.; Wickramasinghe, N. P. *Magn. Reson. Chem.* **2007**, *45*, S221–S230.

(67) Bak, M.; Rasmussen, J. T.; Nielsen, N. C. *J. Magn. Reson.* **2000**, *147*, 296–330.

(68) Deazevedo, E. R.; Saalwachter, K.; Pascui, O.; De Souza, A. A.; Bonagamba, T. J.; Reichert, D. *J. Chem. Phys.* **2008**, *128*, 140505.

(69) Munowitz, M. G.; Griffin, R. G.; Bodenhausen, G.; Huang, T. H. *J. Am. Chem. Soc.* **1981**, *103*, 2529–2533.

18654

dx.doi.org/10.1021/ja203771a |*J. Am. Chem. Soc.* 2011, 133, 18646–18655

(70) Hester, R. K.; Ackerman, J. L.; Neff, B. L.; Waugh, J. S. *Phys. Rev. Lett.* **1976**, *36*, 1081–1083.

(71) Metz, G.; Wu, X. L.; Smith, S. O. *J. Magn. Reson., Ser. A* **1994**, *110*, 219–227.

(72) Baldus, M.; Petkova, A. T.; Herzfeld, J.; Griffin, R. G. *Mol. Phys.* **1998**, *95*, 1197–1207.

(73) Dvinskikh, S. V.; Zimmermann, H.; Maliniak, A.; Sandstrom, D. *J. Magn. Reson.* **2004**, *168*, 194–201.

(74) Destro, R.; Marsh, R. E.; Bianchi, R. *J. Phys. Chem.* **1988**, *92*, 966–973.

(75) Lehmann, M. S.; Koetzle, T. F.; Hamilton, W. C. *J. Am. Chem. Soc.* **1972**, *94*, 2657–2660.

(76) Berthet-Colominas, C.; Monaco, S.; Novelli, A.; Sibai, G.; Mallet, F.; Cusack, S. *EMBO J.* **1999**, *18*, 1124–1136.

(77) Ternois, F.; Sticht, J.; Duquerroy, S.; Krausslich, H. G.; Rey, F. A. *Nat. Struct. Mol. Biol.* **2005**, *12*, 678–682.

(78) Jung, J.; Byeon, I. J. L.; Ahn, J.; Concel, J.; Gronenborn, A. M. *Biomol. NMR Assignments* **2010**, *4*, 21–23.

(79) Marulanda, D.; Tasayco, M. L.; McDermott, A.; Cataldi, M.; Arriaran, V.; Polenova, T. *J. Am. Chem. Soc.* **2004**, *126*, 16608–16620.

(80) Franks, W. T.; Zhou, D. H.; Wylie, B. J.; Money, B. G.; Graesser, D. T.; Frericks, H. L.; Sahota, G.; Rienstra, C. M. *J. Am. Chem. Soc.* **2005**, *127*, 12291–12305.

(81) Igumenova, T. I.; Wand, A. J.; McDermott, A. E. *J. Am. Chem. Soc.* **2004**, *126*, 5323–5331.

(82) Huster, D.; Schiller, J.; Arnold, K. *Magn. Reson. Med.* **2002**, *48*, 624–632.

(83) Lorieau, J. L.; Day, L. A.; McDermott, A. E. *Proc. Natl. Acad. Sci. U.S.A.* **2008**, *105*, 10366–10371.